Superconducting Tunneling and Application

by L. Solymar

Chapter 4
&
Chapter 5

4.3 Junctions between identical superconductors

The energy diagram for $T = 0°K$ is shown in Fig. 4.4. All energy levels are filled up to $E_F - \Delta$. In thermal equilibrium (Fig. 4.4 (*a*)) there is no current flowing. When a voltage $V < 2\Delta/e$ is applied there is still no current flowing because the electrons below the gap on the left have no access to empty states on the right. At $V = 2\Delta/e$ (Fig. 4.4 (*b*)) there is a sudden rise in current because electrons on the left suddenly gain access to the states above the gap on the right. The corresponding current–voltage characteristic is shown in Fig. 4.4 (*c*).

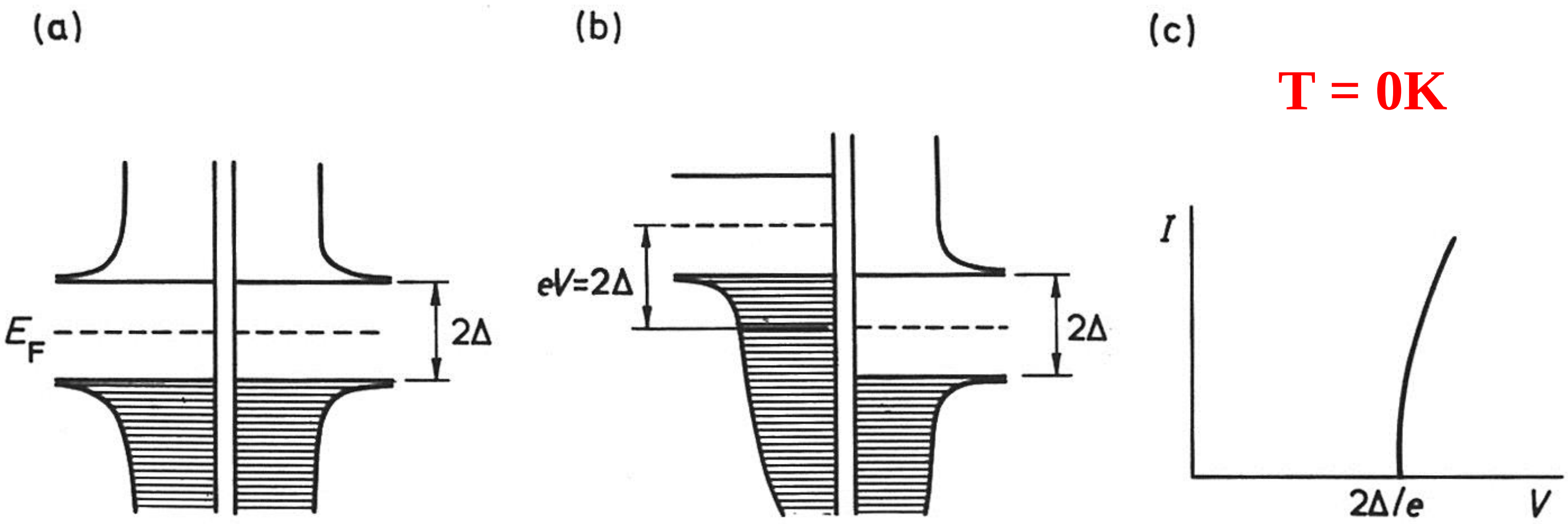

Fig. 4.4 The energy diagram of an SS junction; (*a*) $V = 0$, (*b*) $V = 2\Delta/e$, (*c*) the I–V characteristic at $T = 0$.

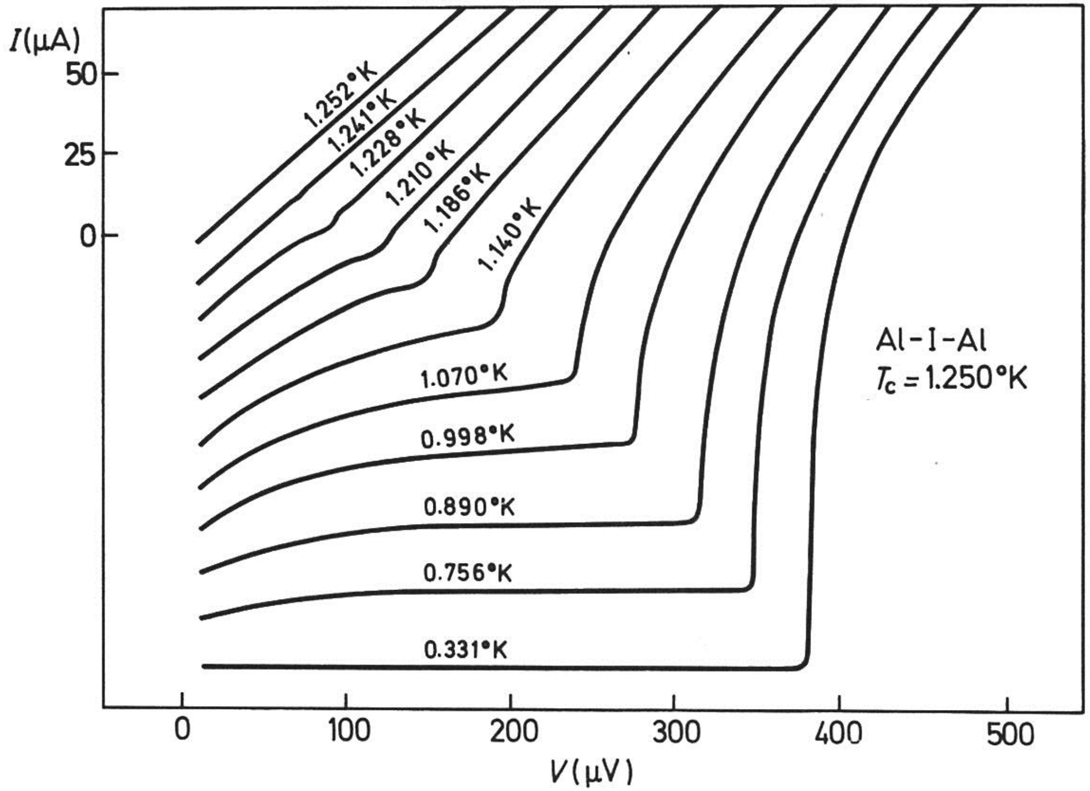

For finite temperatures there will be some rounding off* of the sharp features of Fig. 4.4 (*c*) which, of course, depends on the actual temperature (how near it is to the critical). A very neat set of experimental results (Fig. 4.5) by Blackford and March [99] shows the temperature dependence of the current–voltage characteristic for an aluminium–aluminium oxide–aluminium junction. At 1·252°K aluminium is in the normal state and the characteristic is linear. At 1·241°K (a mere 9 millidegrees below the critical temperature) there is already some sign of the energy gap, and it becomes clearly discernible at 1·228°K. As the temperature decreases the knee in the curves moves to higher and higher voltages (corresponding to higher and higher energy gaps). The characteristic at $T = 0{\cdot}331$°K is practically identical to that at 0°K.

4.4 Junctions between superconductors of different energy gap

In the same way as the previously discussed case of identical superconductors, at $T = 0°K$ no current flows until the applied voltage is sufficiently large to bring the bottom of the gap on the left in line with the top of the gap on the right. This occurs at an applied voltage of $V = (\Delta_1 + \Delta_2)/e$ as shown in Fig. 4.6 (*a*). The current–voltage characteristic (Fig. 4.6 (*b*)) is similar to that shown in Fig. 4.4 (*c*) with the sole difference that the current starts rising at a voltage corresponding to the arithmetical mean of the gap energies.

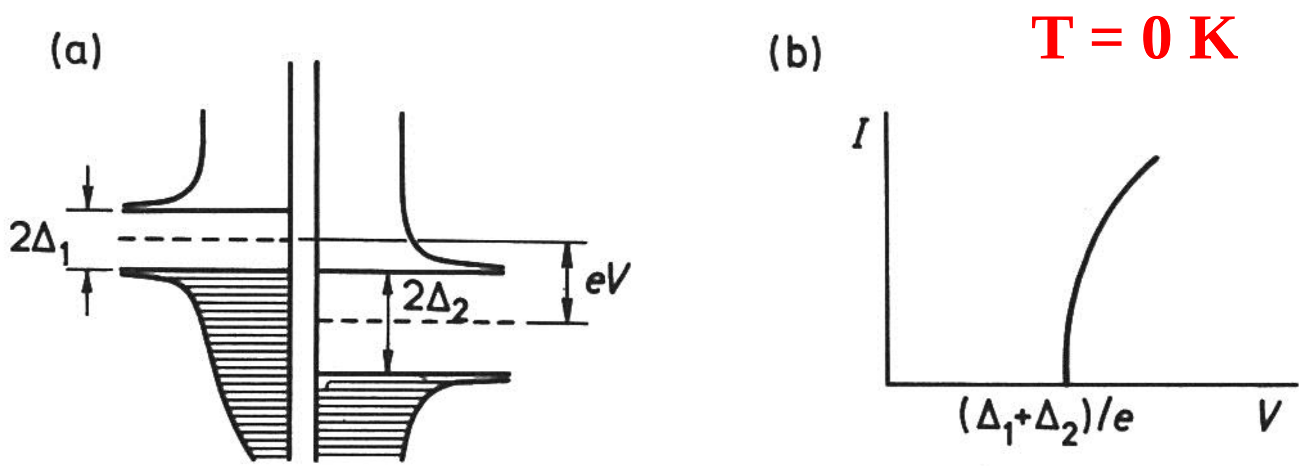

Fig. 4.6 Energy diagram and I–V characteristic of an S_1S_2 junction at $T = 0$.

T > 0K

At finite temperatures we may still assume that the normal electron states above the larger gap are empty but there are some thermally excited normal electrons in the smaller-gap superconductor as shown in Fig. 4.7 (*a*) for the case of thermal equilibrium.

Applying a voltage the current will start to flow immediately and will increase with increasing voltage (Fig. 4.7 (*e*)) until $V = (\Delta_2 - \Delta_1)/e$. The energy diagram for this case is shown in Fig. 4.7 (*b*); at this stage all electrons above the gap on the left can tunnel across into empty states on the right. What happens when the voltage is increased further? The number of electrons capable to tunnel across is still the same but they face a smaller density of states, as shown in Fig. 4.7 (*c*), hence the current decreases. The decrease in current continues until $V = (\Delta_1 + \Delta_2)/e$. At this point (Fig. 4.7 (*d*)) electrons from below the gap on the left gain access to empty states on the right, and there is a sudden increase in current. Thus the current–voltage characteristic of Fig. 4.7 (*e*) exhibits a negative resistance in the region

$$\frac{\Delta_2 - \Delta_1}{e} < V < \frac{\Delta_2 + \Delta_1}{e} \qquad (3.1)$$

T > 0K

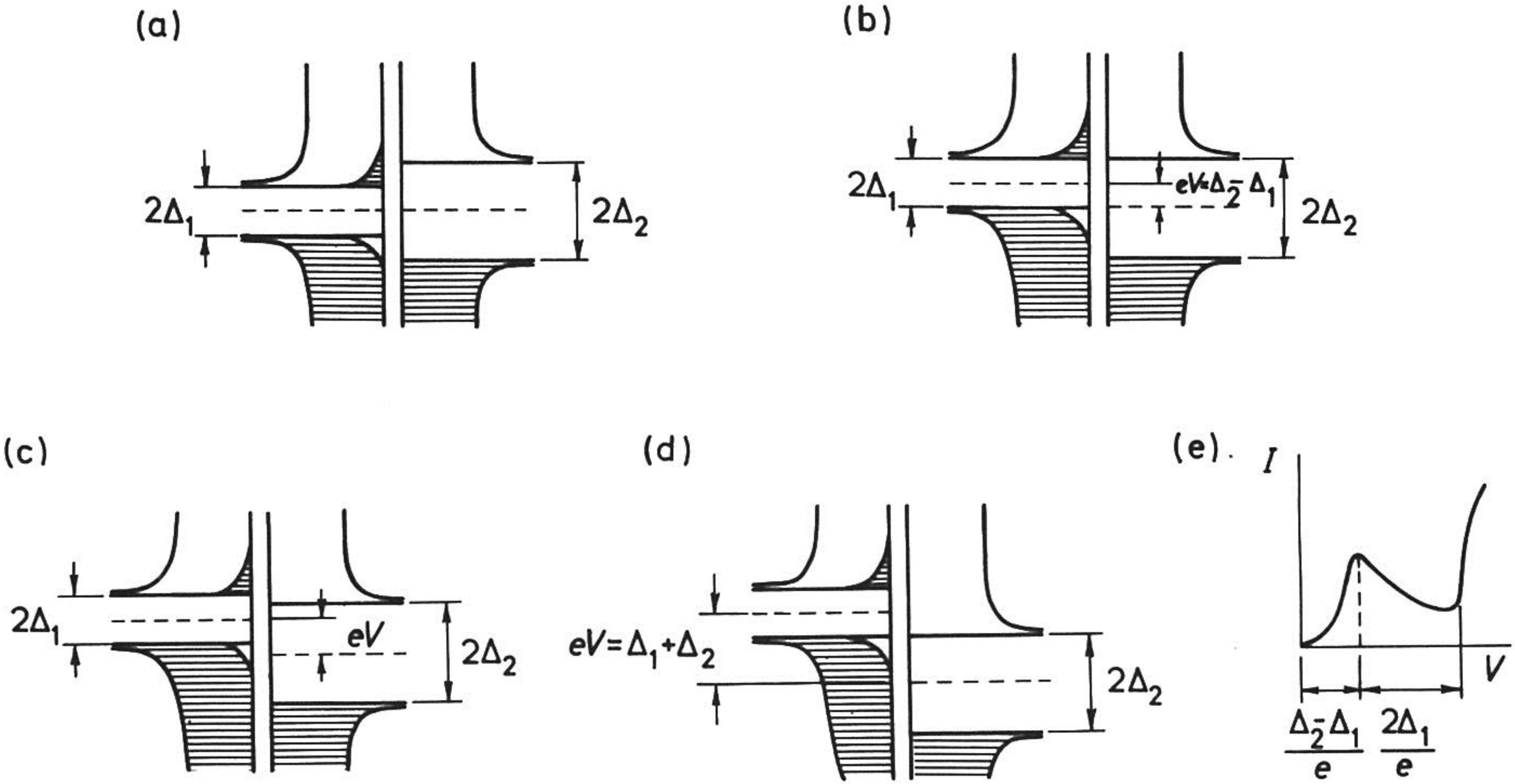

Fig. 4.7 The energy diagram and I–V characteristic of an S_1S_2 junction at finite temperature; (*a*) $V=0$, (*b*) $V=(\Delta_2-\Delta_1)/c$, (*c*) $(\Delta_2-\Delta_1)/e < V < (\Delta_2+\Delta_1)/e$, (*d*) $V=(\Delta_1+\Delta_2)/e$, (*e*) the I–V characteristic.

The appearance of a negative resistance was reported simultaneously by Nicol *et al.* [46] and Giaever [45]. A very convincing characteristic presented by the latter author for an Al–Al_2O_3–Pb junction is shown in Fig. 4.8.

The experimentally found dependence [100] of the negative resistance on temperature is shown in Fig. 4.9 for a Sn–SnO–Pb junction. The current–voltage characteristic turns nonlinear when lead becomes superconducting and the negative resistance appears as soon as tin becomes superconducting as well. The negative resistance may be clearly seen down to 2·39°K but not at 1·16°K. Experimentally the negative resistance always disappears at sufficiently low temperatures but that may be due to insufficient accuracy of measurement and to nonideal circumstances.

The presence of a maximum and minimum in the characteristic gives further help in diagnostic measurements aimed at determining the width of the energy gaps. In addition, the negative resistance may be used in devices which will be discussed in more detail in Section 7.1.

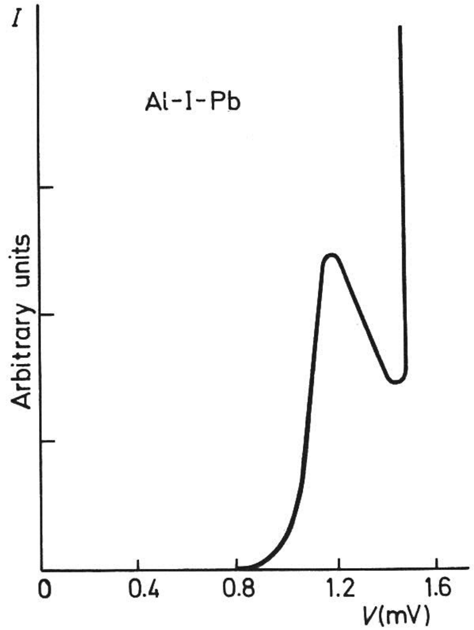

Fig. 4.8 The *I–V* characteristic of an Al–I–Pb junction, both Al and Pb superconducting. After Giaever [45].

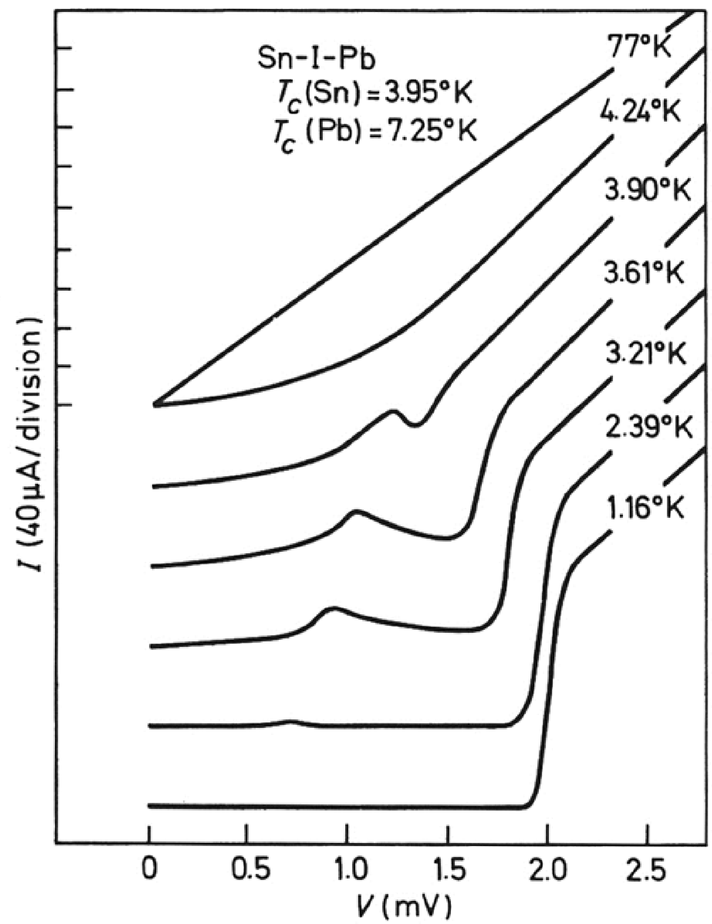

Fig. 4.9 *I–V* characteristics of an Sn–I–Pb junction.

Point contact junctions. These were developed by Levinstein and Kunzler [122, 123] in the form shown in Fig. 4.21. The barrier is prepared by heavily anodising a freshly etched tip of Al, Nb, Ta, etc. The diameter of the junction at the point of contact was estimated to be less than 10 μm. Tunnelling characteristics were observed in a large resistance range from 10^2 to 10^5 ohm.

The advantage of point contacts is that tunnelling measurements can be made on materials not accessible in thin film form. Furthermore, the tunnelling is generally from one single crystal to another since the grain size of the material both in the tip of the point contact and in the bulk is considerably larger than the contact area. Notable success of the point contact technique was to obtain the correct value for the energy gap of Nb_3Sn where thin film measurements consistently gave the wrong value.

was mostly on bulk samples

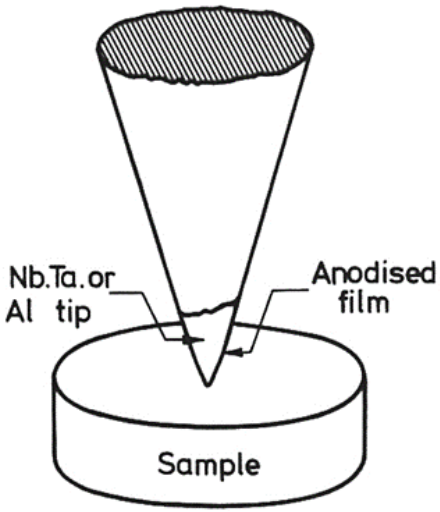

The invention of STM in 1982 !

Fig. 4.21 Point contact junction. After Levinstein and Kunzler [122].

Superconductivity tunneling into the A-15 compounds Nb_3Al, Nb_3Sn, and Nb_3Ge thin film surfaces

Tunneling as a materials diagnosis

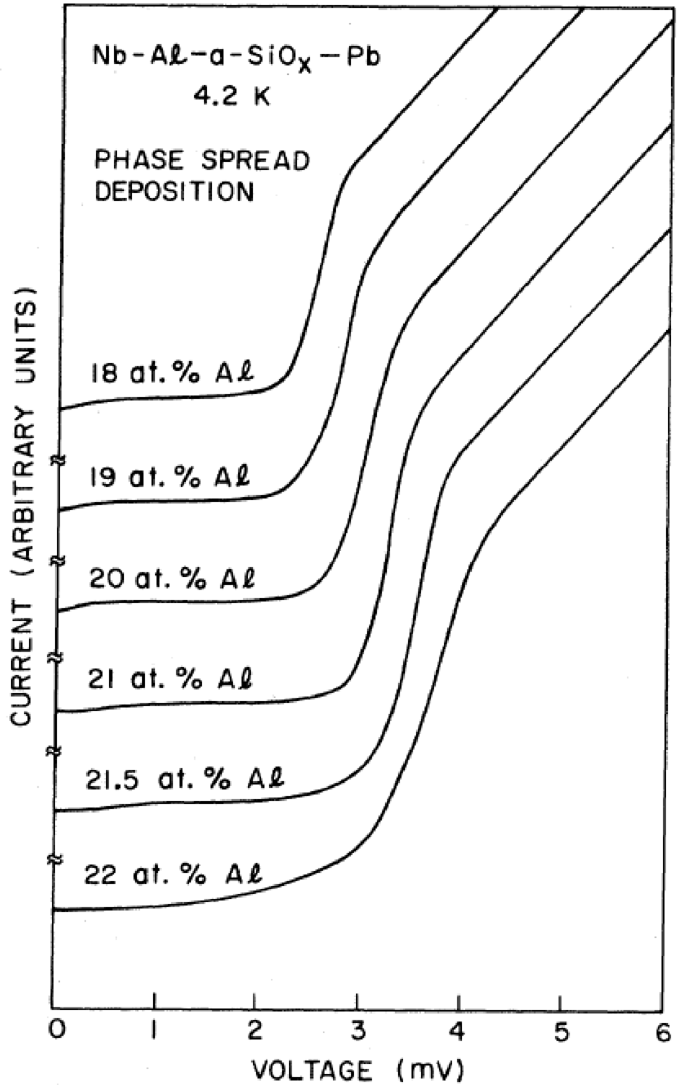

FIG. 2. Current voltage characteristics at 4.2 K of a series of *A*15 Nb-Al junctions obtained from a phase-spread deposition at 950 °C. The thickness of the *a*-Si overlay is of 15 Å. The *A*15 phase boundary is at 21.8 at.% Al.

Tunneling as a materials diagnosis probe

Electron –phonon coupling strength vs composition

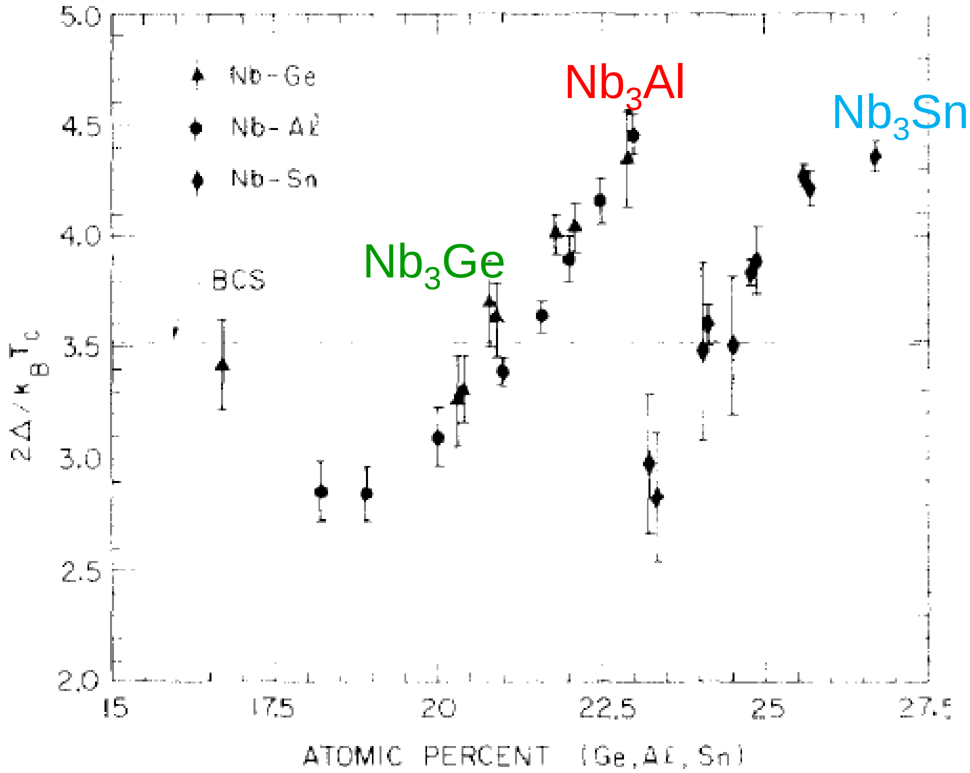

Fig. 2. The variation with composition of the electron–photon coupling strength $2\Delta/k_B T_c$ for the A15 Nb_3Sn, Nb_3Al, and Nb_3Ge. The data are from Rudman et al. [20], Kwo et al. [10], and Khilstrom et al. [11], respectively.

The origin of this dramatic change of the electron-phonon coupling strength of Nb_3Al with the composition approaching the $A15$ phase boundary is not well understood. An insight can be gained from referring to the analytical formula by Kresin *et al.*,[21]

$$\boxed{2\Delta/k_B T_c = 3.53[1+5.3(T_c/\omega_0)^2 \ln(\omega_0/T_c)] \quad ,}$$

which expresses the enhancement of the coupling strength $2\Delta/k_B T_c$ as an explicit function of the ratio T_c/ω_0, where ω_0 is a characteristic Einstein phonon frequency. An analysis based on this formula shows that a change in the $2\Delta/k_B T_c$ ratio from BCS-like to a value as large as 4.4 requires a substantial increase in T_c/ω_0. Since T_c varies only modestly, from 14.0 to 16.4 K, the occurrence of phonon-mode softening, i.e., a smaller ω_0, appears necessary to account for the large increase in T_c/ω_0. The most direct proof of this supposition is to examine the $\alpha^2 F(\omega)$ functions states.
obtained experimentally from tunneling densities of

E. Tunneling density of states and $\alpha^2F(\omega)$

The dynamic resistance dV/dI as a function of the bias voltage has been measured for several Nb-Al junctions of importance. Data of the superconducting state were taken at 1.5 K with a magnetic field ~1 kG applied to quench the superconductivity in Pb. Throughout the data reduction, a constant excess conductance, of about 2–5% of the normal-state conductance, was subtracted out from both the superconducting and the normal-state tunneling conductance. The energy gap Δ was determined experimentally with the aid of Bermon's table.[22] The reduced tunneling density of states $R(\omega)=N_{expt}(\omega)/N_{BCS}(\omega)-1$ was then calculated. Figure 6 shows

- Reduced tunneling density of states $R(\omega)$, $R(\omega) = N_{exp}(\omega) / N_{BCS}(\omega) -1$
- *Use $R(\omega)$ and Δ to deduce to $\alpha^2F(\omega)$ by the MR inversion program to deduce λ and μ^**
- *Use the MMR inversion program to include a normal proximity layer with d, l, and v_F*

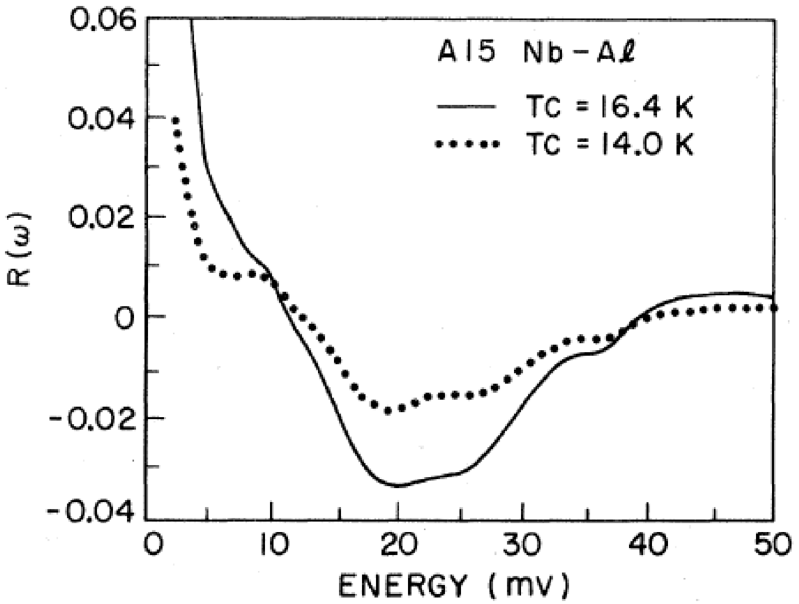

FIG. 6. Reduced tunneling density of states $R(\omega)$ vs energy above the gap for the two Nb-Al junctions of $T_c=16.4$ K, $\Delta=3.15$ meV and $T_c=14.0$ K, $\Delta=2.15$ meV, respectively.

The electron-phonon spectral function $\alpha^2 F(\omega)$ has

been generated from the input data of $R(\omega)$ and Δ by the gap-inversion analysis for these two junction The initial method employed was the conventional McMillan-Rowell inversion program.[24] For the jun tion with a T_c of 16.4 K and a Δ of 3.15 meV, that analysis gives a value of only 0.6 for the electron-phonon interaction parameter λ and a negative valu ~ -0.10 for the effective Coulomb pseudopotential μ^*. The calculated T_c from these parameters is thu less than 10 K. Perhaps the most unphysical result using that analysis is that a high-energy cutoff of le than 30 meV had to be imposed to prevent the iter tive solutions from becoming unstable. The structu between 20 and 40 meV, as associated with the Al phonons, was then left out entirely. Furthermore, shown in Fig. 7, there is a large positive offset between the experiment and the calculated $R(\omega)$'s.

modified McMillan-Rowell (MMR) inversion analysis based on the model of proximity-effect tunneling, proposed by Arnold[26] and implemented by Wolf *et al.*,[27] has permitted an improved description, i.e., more self-consistent, of the tunneling data of such Nb and Nb_3Sn junctions within the conventional framework of the strong-coupling theory.[28,29] In this model a thin layer of weakened superconductivity is proposed to exist between the insulating oxide and the base electrode, and it is characterized by a constant pair potential $\Delta_n << \Delta_s$ and a thickness of $d_n << \xi$.

It is plausible that a thin proximity layer exists between the Nb_3Al film and the *a*-Si oxide barrier. It

With no *a priori* knowledge about this promixity layer, we approximate it with $\Delta_n = 0$. The tunneling density of states is then, as shown in Ref. 26, dependent on two additional parameters, $2d_n/\hbar v_F^*$ and d_n/l, where d_n, v_F^*, and l are the thickness, the renormalized Fermi velocity, and the mean free path of the promiximity layer, respectively.

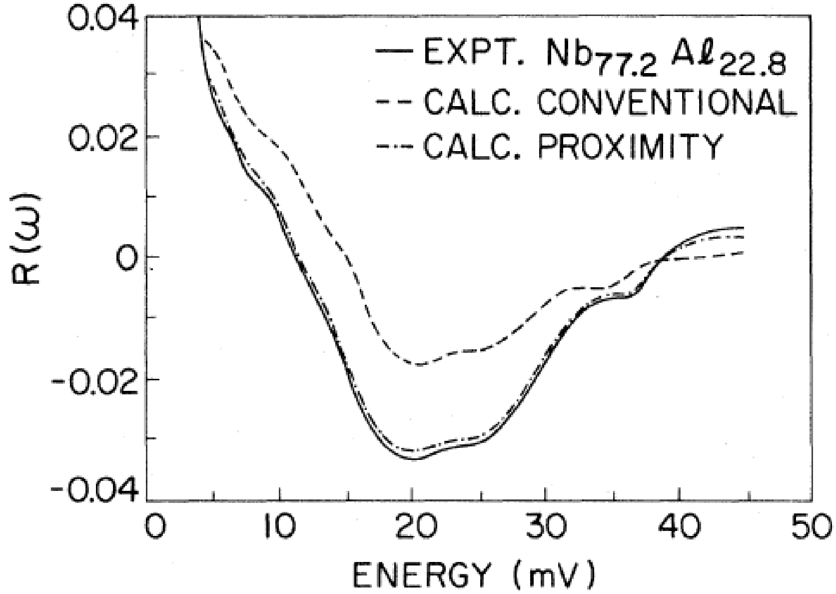

FIG. 7. The experimental and calculated tunneling densities of states $R(\omega)$'s from both conventional and proximity inversion analysis for the $A15$ Nb-Al junction of 22.8 at.% Al with $T_c = 16.4$ K and $\Delta = 3.15$ meV.

reduced tunneling density of states $R(\omega) = N_{\mathrm{expt}}(\omega)/N_{\mathrm{BCS}}(\omega) - 1$ was then calculated. Figure 6 shows the $R(\omega)$'s for two particular junctions. One is a relatively weak coupled superconductor, with a T_c of 14.0 K and a gap of 2.15 meV; the other is strong coupled, of larger Al composition by 1.3 at.%, with a higher T_c at 16.4 K and a gap of 3.15 meV. A reduction in the magnitude of $R(\omega)$ is found as the Al composition is reduced, indicating a weakening in the electron-phonon coupling strength. However, the overall shapes of the two $R(\omega)$'s are rather similar, and there is no dramatic change in the positions of structures induced by phonons. Similar behavior is found in the tunneling densities of states of Nb_3Sn junctions of different T_c's and coupling strength.[23]

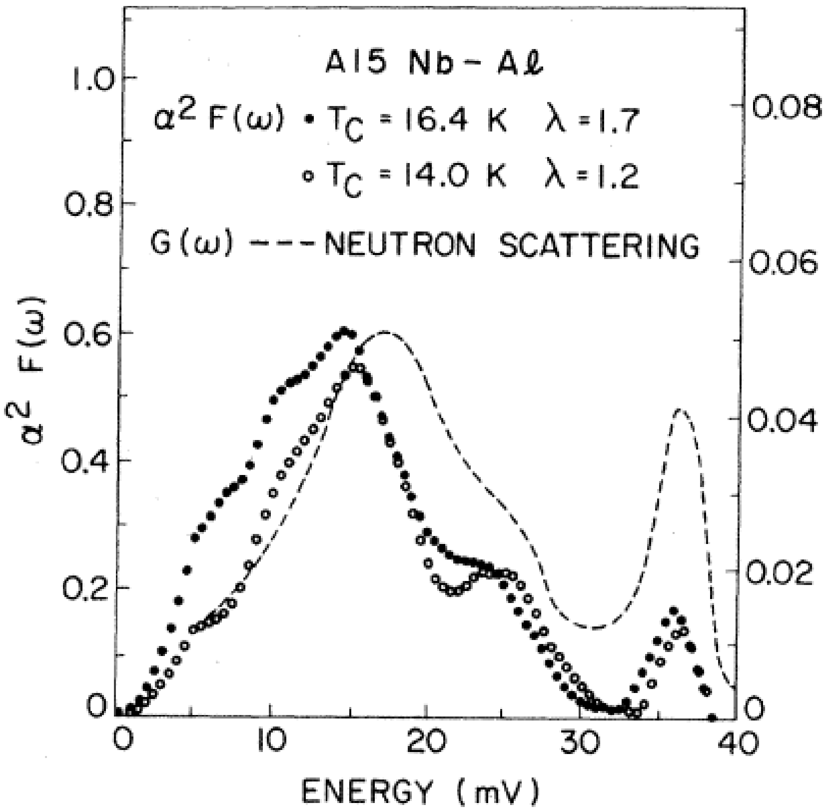

FIG. 8. The electron phonon spectral functions $\alpha^2 F(\omega)$ for two Nb-Al junctions with $2\Delta/k_B T_c$ of 3.6 and 4.4. The data of the neutron scattering function $G(\omega)$ are after Schweiss *et al.* (Ref. 9).

features of the $\alpha^2 F(\omega)$ functions of these two junctions are quite similar, with a slight reduction of about 10% in the $\alpha^2 F_{max}$ for the lower-T_c one. However the strong-coupled and high-T_c junction shows a pronounced enhancement in the weightings of the low-frequency phonons, leading to smaller values of the frequency moments. In fact, the significant reduction of λ, from 1.7 to the 1.2 found for the lower-T_c junction, is mainly from the stiffening of phonons; i.e., $\langle \omega^2 \rangle$ is larger by 20%. The $\alpha^2 F(\omega)$

$$T_c = \frac{\Theta_D}{1.45} \exp\left\{-\left[\frac{(1+\lambda_{ep})}{\lambda_{ep} - \mu^*(1+0.62\lambda_{ep})}\right]\right\}$$

to the analytical formula by Kresin *et al.*,[21]

$$2\Delta/k_B T_c = 3.53[1 + 5.3(T_c/\omega_0)^2 \ln(\omega_0/T_c)] \quad ,$$

which expresses the enhancement of the coupling strength $2\Delta/k_B T_c$ as an explicit function of the ratio T_c/ω_0, where ω_0 is a characteristic Einstein phonon frequency.

[a] $\lambda = 2\int d\omega\, \omega^{-1} \alpha^{a} F(\omega)$.

[b] $\omega_{\log} = \exp\left[\frac{2}{\lambda} \int d\omega\, \omega^{-1} \ln\omega\, \alpha^2 F(\omega)\right] \quad .$

[c] $T_c = \frac{\langle\omega\rangle}{1.2} \exp\left[\frac{-1.04(1+\lambda)}{\lambda - \mu^*(1+0.62\lambda)}\right]$, see Ref. 30.

$\lambda = N(0)\langle I^2\rangle / M \langle\omega^2\rangle$

The electron–phonon coupling constant λ can be expressed, according to McMillan, as a product of $\boxed{N^{b}(0)\langle I^2\rangle/M\langle\omega^2\rangle}$ where $N^{b}(0)$ and $\langle I^2\rangle$ are the electronic band density of states and the electron–phonon matrix element evaluated over the Fermi surface, respectively. The electronic parameter $N^{b}(0)$ can be estimated from the renormalized density of states $N^{*}(0)$ by specific

(1) or (2)

heat experiments or from upper critical field analysis, given that the $(1+\lambda)$ factor is known from tunneling. Systematic variations of these

$$C_{el} = 1/3\ \pi^2 N(0) K_B^2\ T$$

$$\boxed{N^{b}(0)\left(\frac{\text{states}}{\text{eV spin unit cell}}\right) = \frac{17.8}{1+\lambda}\gamma^{*M}\left(\frac{\text{mJ}}{\text{cm}^3\text{K}^2}\right),}$$

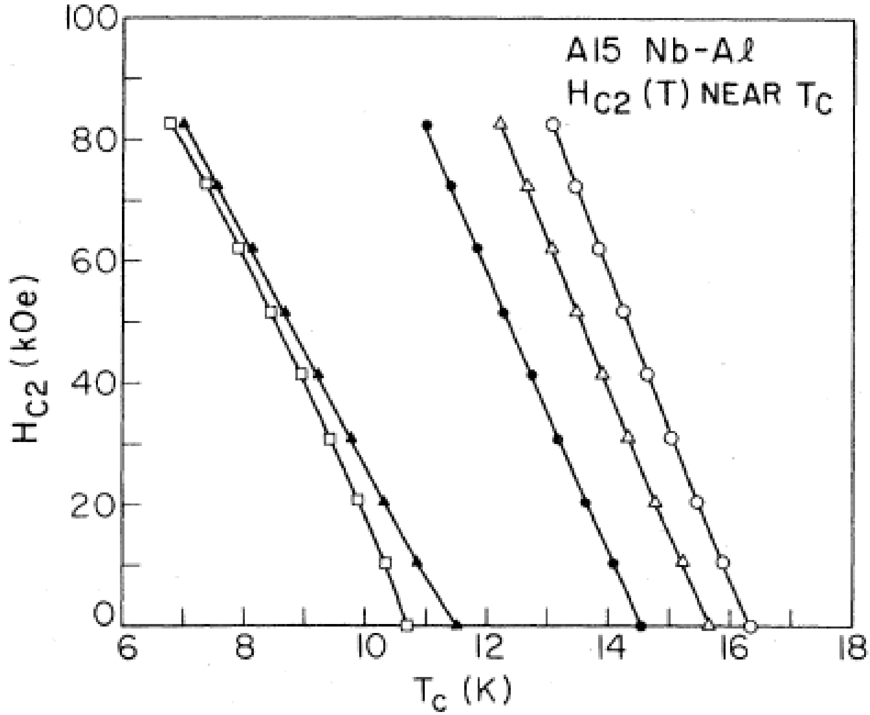

FIG. 1. Representative critical-field data near T_c of the A15 Nb-Al films measured. The lines drawn through data points are intended to serve only as a guide to the eye.

Based on the data of the critical-field slope near T_c, the general procedure of evaluating various superconducting and normal-state parameters including $N^b(0)$ is well formulated.[20] Briefly, the slope of critical field near T_c including corrections for the electron-phonon interaction can be written as[21]

$$\left.\frac{dH_{c2}}{dT}\right|_{T_c} = \eta_{H_{c2}}(T_c)\left[9.55\times10^{24}\gamma^{*2}T_c\left(\frac{n^{3/2}S}{S_F}\right)^{-2} + 5.26\times10^{4}\gamma^{*}\rho(\Omega\,\mathrm{cm})\right]\times[R(\gamma_{\mathrm{tr}})]^{-1}\ \mathrm{Oe/K}\ ,$$

Nb tunnel junctions for Josephson device applications

Nb/Al/oxide/Pb junctions

Nb JOSEPHSON TUNNEL JUNCTIONS WITH THIN LAYERS
OF Al NEAR THE BARRIER

M. Gurvitch, J. M. Rowell, H. A. Huggins,
M. A. Washington and T. A. Fulton

Bell Laboratories
Murray Hill, New Jersey 07974

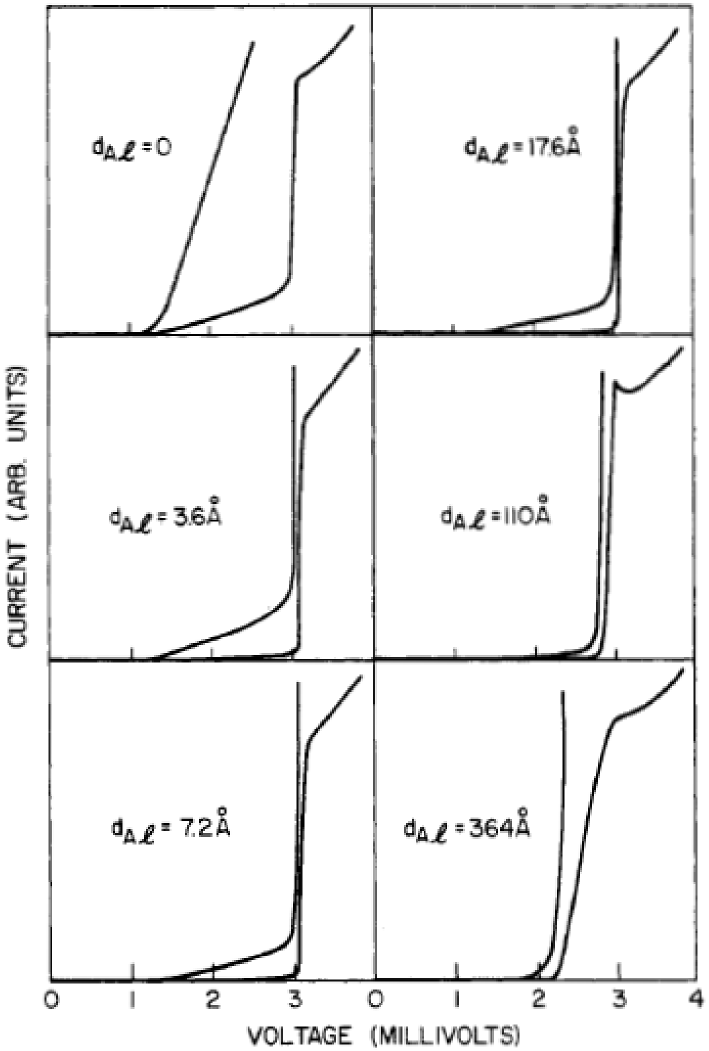

Fig. 2 Volt-ampere characteristics of Nb/Al-oxide-$Pb_{0.90}Bi_{0.10}$ junctions with different d_{Al} at $T \cong 2^oK$. Expansion of the current scale ×10 is also shown. The junction without an Al overlayer was oxidized for 4 days, the rest for 20 min. All junctions have area $S \cong 2\cdot10^{-3}$ cm^2.

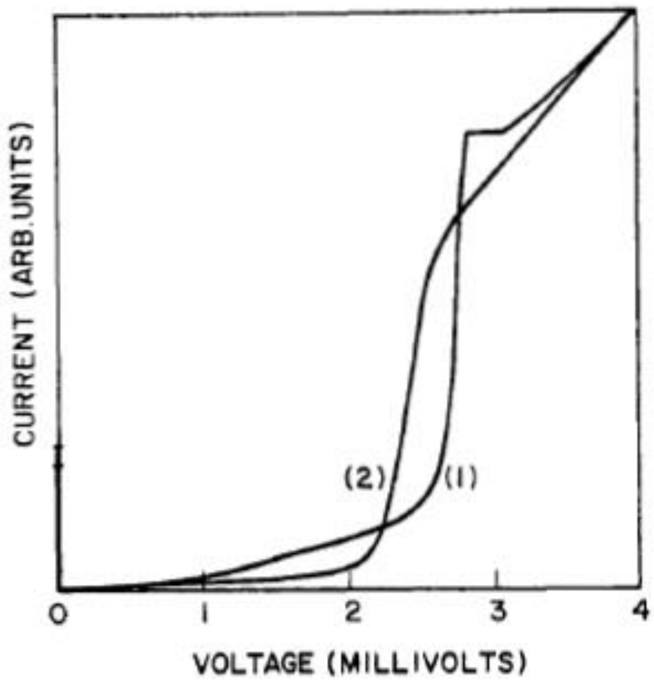

Fig. 3 Volt-ampere characteristics of Nb/Al-oxide-Nb (curve 1) and Nb/Al-oxide-Al/Nb (curve 2) junctions at $T \cong 2^oK$. Both base electrodes have d_{Al} = 25Å, the top electrode of the junction with the second Al layer has d_{Al} = 32Å. Critical currents are ~50A/cm^2.

IEEE TRANSACTIONS ON MAGNETICS, VOL. MAG-19, NO. 3, MAY 1983

XPS and Tunneling Study of Air-oxidized Overlayer Structures of Nb with Thin Mg, Y and Er

J. Kwo
G. K. Wertheim
M. Gurvitch
D. N. E. Buchanan

Bell Laboratories
Murray Hill, New Jersey 07974

Artificial tunnel barrier made of oxides of thin Si, Mg, Y, and Er

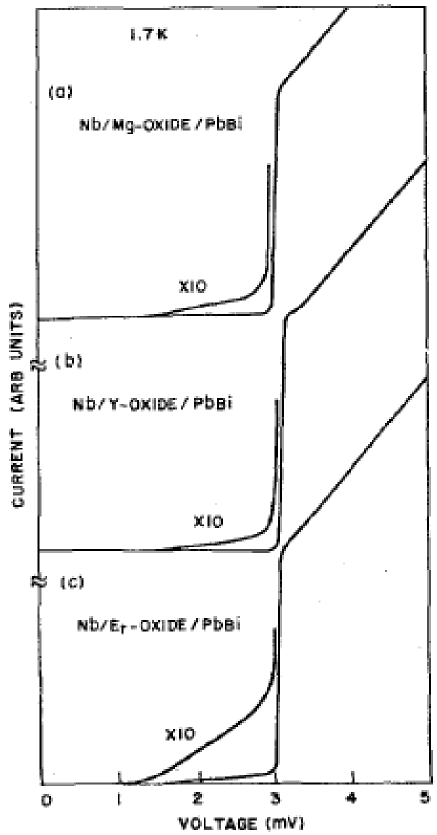

Fig. 2 Current-voltage characteristic of junctions of
(a) Nb/16.6Å Mg-oxide/$Pb_{0.9}Bi_{0.1}$, R = 21.7 Ω
(b) Nb/Y 8.7Å Y-oxide/$Pb_{0.9}Bi_{0.1}$, R = 181 Ω
(c) Nb/Er 4.5Å Er-oxide/$Pb_{0.9}Bi_{0.1}$, R = 20 Ω
The junction area is typically of 1.3×10^{-2}cm^2.

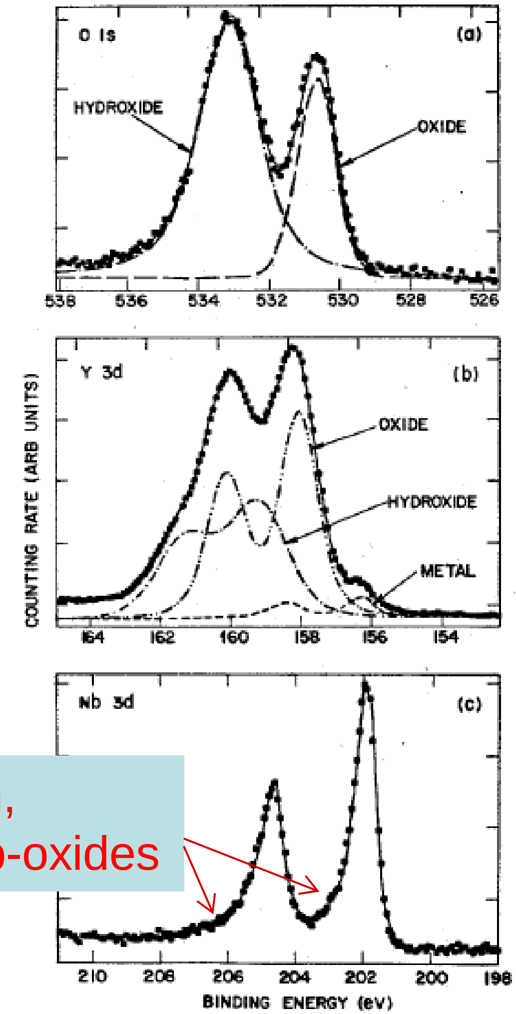

Very clean,
free of sub-oxides

Fig. 3 XPS data for a sample of Nb/30Å Y overlayer
(a) 0 1s
(b) Y 3d
(c) Nb 3d

References

PHYSICAL REVIEW B | VOLUME 23, NUMBER 7 | 1 APRIL 1981

Superconducting tunneling into the *A*15 Nb_3Al thin films

J. Kwo and T. H. Geballe*
Department of Applied Physics, Stanford University, Stanford, California 94305

PHYSICAL REVIEW B | VOLUME 24, NUMBER 5 | 1 SEPTEMBER 1981

Microscopic superconducting parameters of Nb_3Al: Importance of the band density of states

J. Kwo,* T. P. Orlando,† and M. R. Beasley‡
Department of Applied Physics, Stanford University, Stanford, California 94305
(Received 12 December 1980)

PHYSICAL REVIEW B | VOLUME 24, NUMBER 4 | 15 AUGUST 1981

Modification of tunneling barriers on Nb by a few monolayers of Al

J. M. Rowell, M. Gurvitch, and J. Geerk*
Bell Laboratories, Murray Hill, New Jersey 07974
(Received 10 June 1981)

VOLUME 63, NUMBER 9 | PHYSICAL REVIEW LETTERS | 28 AUGUST 1989

Reproducible Tunneling Data on Chemically Etched Single Crystals of $YBa_2Cu_3O_7$

M. Gurvitch, J. M. Valles, Jr., A. M. Cucolo,[a] R. C. Dynes, J. P. Garno, L. F. Schneemeyer, and J. V. Waszczak
AT&T Bell Laboratories, Murray Hill, New Jersey 07974
(Received 26 May 1989)

Observations of quasi-particle tunneling and Josephson behavior in $Y_1Ba_2Cu_3O_{7-x}$/native barrier/Pb thin-film junctions
J. Kwo, T. A. Fulton et al, Appl. Phys. Lett. **56**, 788 (1990).

5.2 Photon-assisted tunnelling

The tunnelling current may be modified by illuminating the junction with electromagnetic waves. It is easy to see that if the energy of the incident photons is in excess of 2Δ they will break up Cooper-pairs and create two electrons above the gap as shown in Fig. 5.5 (*a*). Since the number of electrons above the gap increases this way above its equilibrium value, some of these extra electrons will tunnel across the barrier (Fig. 5.5 (*b*)) creating thereby an extra current. We shall return to this problem in Section 7.2, for the moment we shall concentrate on the case when the energy of the incident photon is insufficient to break up a Cooper-pair. Influence on the tunnelling characteristics is still possible then if the photons act jointly with the applied voltage.

T = 0K

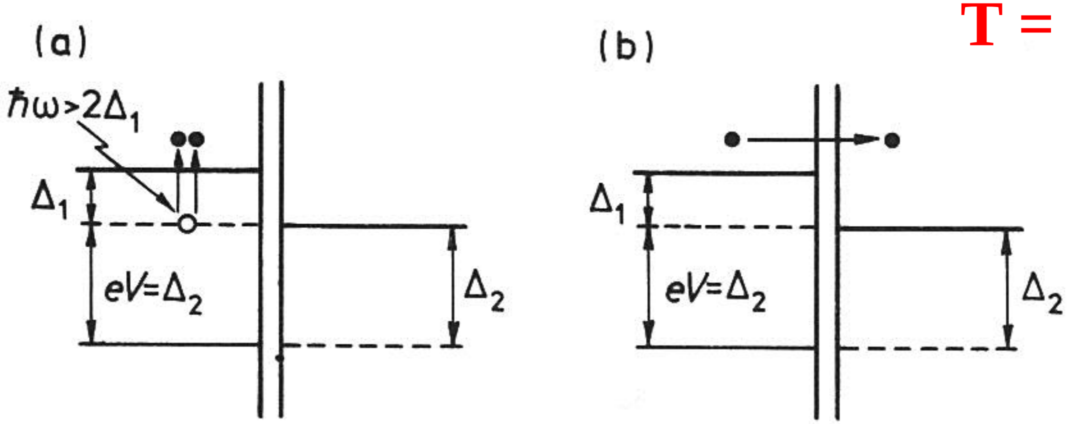

Fig. 5.5 Effect of incident photons on a tunnel junction; (*a*) a photon creates two electrons by breaking up a Cooper-pair, (*b*) one of the electrons created tunnels across.

Let us take $T = 0°K$ again and recall the case when $V = (\Delta_1 + \Delta_2)/e$. Then a Cooper-pair may break up into two electrons, one of them tunnelling across the barrier as has been shown in Fig. 4.12. If $V < (\Delta_1 + \Delta_2)/e$ no current flows. A Cooper-pair breaking up could not cause a current because the transition shown in Fig. 5.6 (*a*) with dotted lines is not permissible. However, if a photon of the right energy is available the liberated electron may follow the path shown in Fig. 5.6 (*b*) and get into an allowed state just above the gap. We may say that the electron tunnelled across the barrier by absorbing a photon, and refer to the phenomenon as photon-assisted tunnelling. The mathematical condition for the onset of tunnelling current is

for $eV < \Delta_1 + \Delta_2$

$$\hbar\omega = \Delta_1 + \Delta_2 - eV. \qquad (5.1)$$

T = 0K

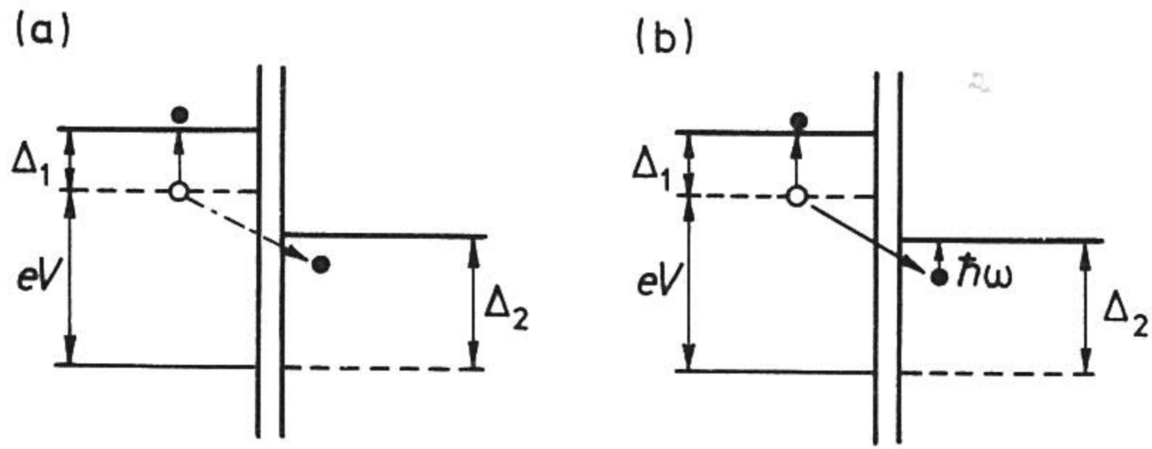

Fig. 5.6 (*a*) Tunnelling not allowed. (*b*) Tunnelling allowed if assisted by a photon.

If the energy of the photon is above this value tunnelling is still possible, though with a reduced probability because of a less favourable density of states. If the energy of the incident photon is below the value given by Equation (5.1) tunnelling may still be possible with the aid of a multi-photon process. An electron absorbing for example three photons simultaneously may tunnel across the barrier in the way shown in Fig. 5.7 (*a*). Hence we may expect sudden rises in the tunnelling characteristics whenever the condition

$$n\hbar\omega = \Delta_1 + \Delta_2 - eV \tag{5.2}$$

is satisfied, that is for a series of voltages in the range $0 < V < (\Delta_1 + \Delta_2)/e$.

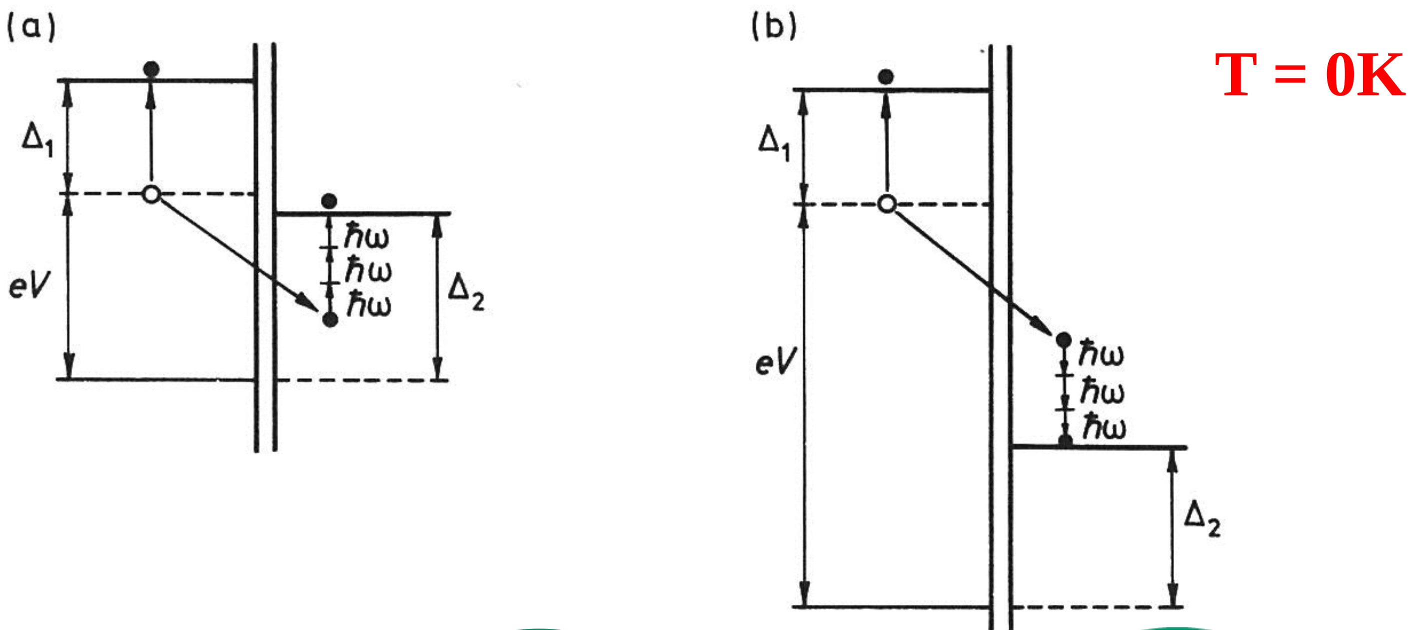

Fig. 5.7 Tunnelling assisted (*a*) by absorption of three photons, (*b*) by emission of three photons.

For eV > $\Delta_1 + \Delta_2$

When $V > (\Delta_1 + \Delta_2)/e$ we know that a tunnelling current will flow even in the absence of an incident electromagnetic wave. However, if photons of the right energy are available they can assist the tunnelling in this case as well, as shown in Fig. 5.7 (*b*) for a three-photon process. A Cooper-pair breaks up; one of the electrons goes into a state just above the gap on the left, and the other electron tunnels across into the superconductor on the right at an energy demanded by energy conservation (the sum of electron energies must equal the energy of the Cooper-pair). This process would occur with much higher probability if the electron could tunnel into the high density states lying just above the gap on the right. In Fig. 5.7 (*b*) this becomes energetically possible when three photons are *emitted* at the same time. Thus the mechanism of current rise is photon emission *stimulated* by input photons. For an *n*-photon emission process the current rises occur when

T = 0K

$$V_n = \frac{1}{e}(\Delta_1 + \Delta_2 + n\hbar\omega). \tag{5.3}$$

T > 0K

For finite temperatures there is one more instance where electrons tunnel between maximum density states and that occurs $\boxed{\text{at } V = (\Delta_2 - \Delta_1)/e,}$ as shown in Fig. 5.8 (*a*). Tunnelling between those states may also be assisted by photons as shown in Figs. 5.8 (*b* and *c*) for photon absorption and emission respectively. In general, multi-photon absorptions and emissions are possible again, and thus for finite temperatures there is another set of voltages,

$$\boxed{V_\mathrm{m} = \frac{1}{e}(\Delta_2 - \Delta_1 + m\hbar\omega), \qquad m = \pm 1, \pm 2, \pm 3} \tag{5.4}$$

at which current rises can be expected.

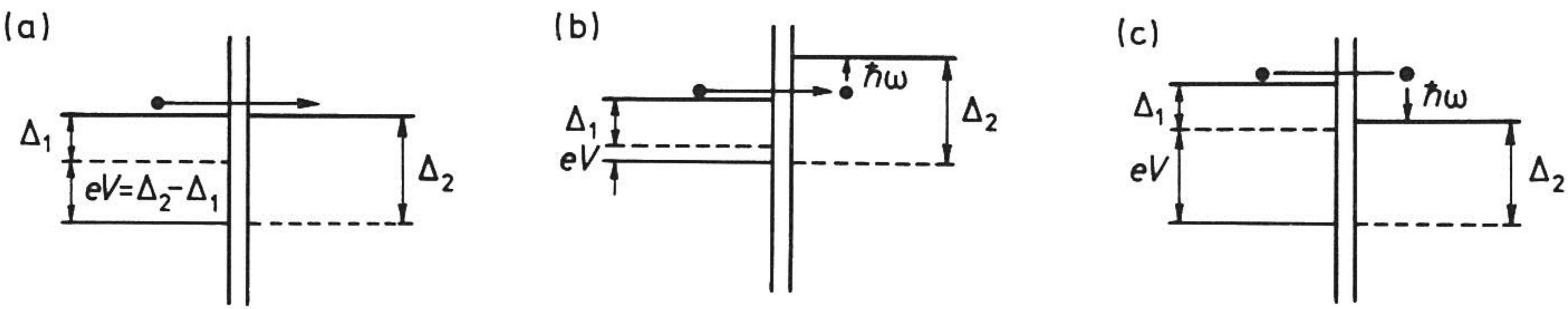

Fig. 5.8 Tunnelling between maximum density states at finite temperature (*a*) directly, (*b*) by photon absorption, (*c*) by photon emission.

The first experiments on tunnel junctions in the presence of electromagnetic waves were performed by Dayem and Martin [57] using junctions between Al and Pb, In or Sn. The frequency of the electromagnetic wave employed was 38·83 GHz so the experimental solution was to place the sample inside a cavity. The current–voltage characteristic was measured and rises in current were indeed found as may be seen in Fig. 5.9 (*a*) where the solid and dotted lines show the characteristic in the absence and presence of microwaves respectively.

Quantitative explanations were given nearly simultaneously by Tien and Gordon [58] and Cohen, Falicov and Phillips [126]. The methods in their papers were different but obtained essentially the same results. Cohen, Falicov and Phillips assumed that the magnetic field of the microwaves modulates the energy gap, whereas Tien and Gordon added an electrostatic perturbation term to the Hamiltonian. We shall follow here the latter derivation.

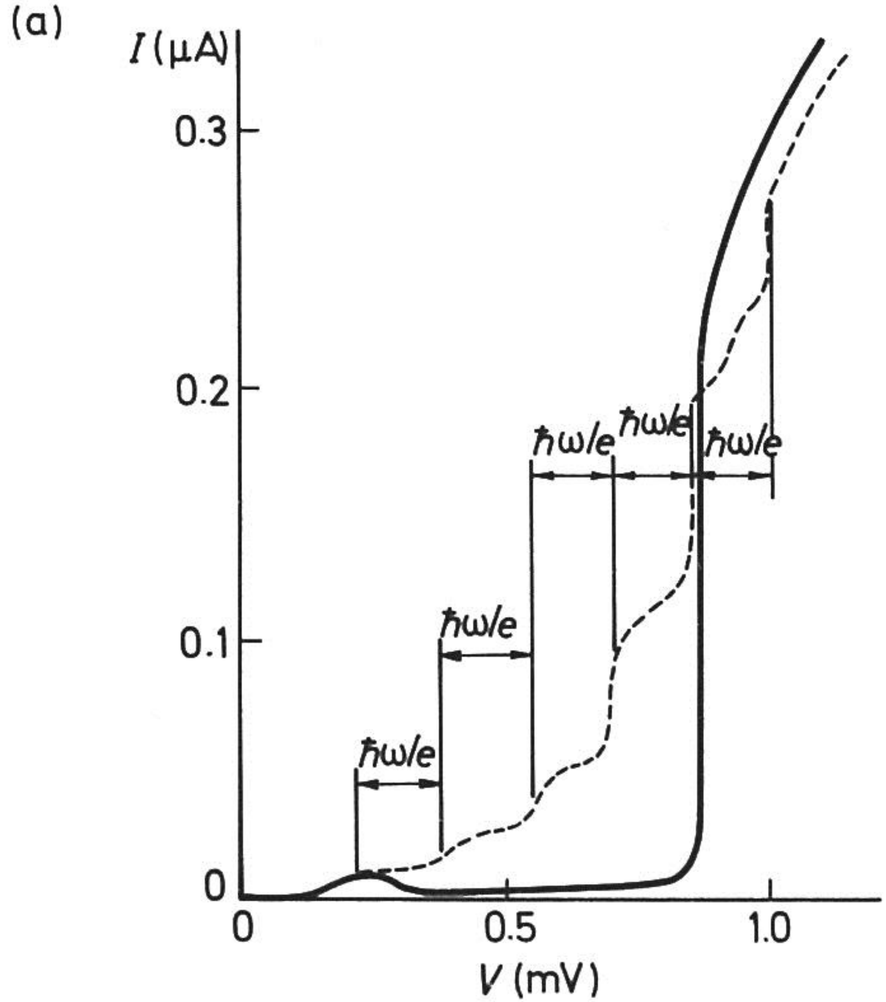

Fig. 5.9 (*a*) *I–V* characteristic of an Al–I–In junction in the absence (solid lines) and presence (dotted lines) of microwaves of frequency 38·83 GHz. Measurements by Dayem and Martin, quoted by Tien and Gordon [58].

The simplest assumption one can make is to regard the junction as a capacitance with a time-varying but spatially constant electric field between the plates. Regarding the potential of one of the superconductors (2) as the reference we may argue that the only effect of the microwave field is to add an electrostatic potential of the form

$$V_{\mathrm{rf}} \cos \omega t \tag{5.5}$$

to the energy of the electrons in the other superconductor (1). Hence, for electrons in superconductor (1) we may use the new Hamiltonian

$$H = H_0 + eV_{\mathrm{rf}} \cos \omega t \tag{5.6}$$

where the first term is the unperturbed Hamiltonian in the absence of microwaves.

If the unperturbed wavefunction was

$$\Psi_0(x, y, z, t) = f(x, y, z) \exp(-iEt/\hbar) \tag{5.7}$$

then the solution for the new wavefunction may be sought in the form

$$\boxed{\Psi(x, y, z, t) = \Psi_0(x, y, z, t) \sum_{n=-\infty}^{\infty} B_n \exp(-in\omega t).} \tag{5.8}$$

Substituting Equation (5.8) into Schrödinger's equation

$$H\Psi = i\hbar\frac{\partial\Psi}{\partial t} \tag{5.9}$$

we find

$$2nB_n = \frac{eV_{\mathrm{rf}}}{\hbar\omega}(B_{n+1} + B_{n-1}) \tag{5.10}$$

which is satisfied by [101]

$$B_n = J_n(eV_{\mathrm{rf}}/\hbar\omega) \tag{5.11}$$

where J_n is the n_{th} order Bessel function of the first kind. The new wavefunction is then

$$\Psi(x, y, z, t) = f(x, y, z, t)\exp(-iE\hbar/t)\sum_{n=-\infty}^{\infty} J_n(\alpha)\exp(-in\omega t), \tag{5.12}$$

where

$$\alpha = \frac{eV_{\mathrm{rf}}}{\hbar\omega}. \tag{5.13}$$

It may be seen that in the presence of microwaves the wavefunction contains components with energies

$$E, E \pm \hbar\omega, E \pm 2\hbar\omega, \ldots \tag{5.14}$$

respectively. Without the electric field, an electron of energy E in superconductor (1) can only tunnel to the states in superconductor (2) of the same energy. In the presence of the electric field, the electron may tunnel to the states in superconductor (2) of energies E, $E \pm \hbar\omega$, $E \pm 2\hbar\omega$, etc. Let $N_{20}(E)$ be the unperturbed density of states of the superconductor (2). In the presence of microwaves we then have an effective density of states given by

$$N_2(E) = \sum_{n=-\infty}^{\infty} N_{20}(E + n\hbar\omega) J_n^2(\alpha). \tag{5.15}$$

We may now obtain the tunnelling current by substituting Equation (5.15) into the general expression Equation (2.14), yielding*

$$I = A \sum_{n=-\infty}^{\infty} J_n^2(\alpha) \int_{-\infty}^{\infty} N_1(E-eV)N_{20}(E+n\hbar\omega)[f(E-eV)-f(E+n\hbar\omega)]\,dE$$

$$= A \sum_{n=-\infty}^{\infty} J_n^2(\alpha) I_0(eV+n\hbar\omega) \tag{5.16}$$

where $I_0(eV)$ is the tunnelling current in the absence of microwaves.

In the limit $\hbar\omega \to 0$ it may be shown (see Appendix 5) that the above expression reduces to the classical value

$$I = \frac{1}{\pi} \int_{-\pi/2}^{\pi/2} I_0(V + V_{\mathrm{rf}} \sin \omega t)\, d(\omega t). \tag{5.17}$$

The comparison between theory and experiments has a long and tangled story. The first attempt was made by Tien and Gordon [58] who could reproduce the experimental results of Dayem and Martin [57] by taking $\alpha = 2$ as shown in Fig. 5.9 (*b*). The experimental value of α (that is the voltage in the junction) was, however, not known. Estimates by Tien and Gordon indicated a discrepancy as large as an order of magnitude.

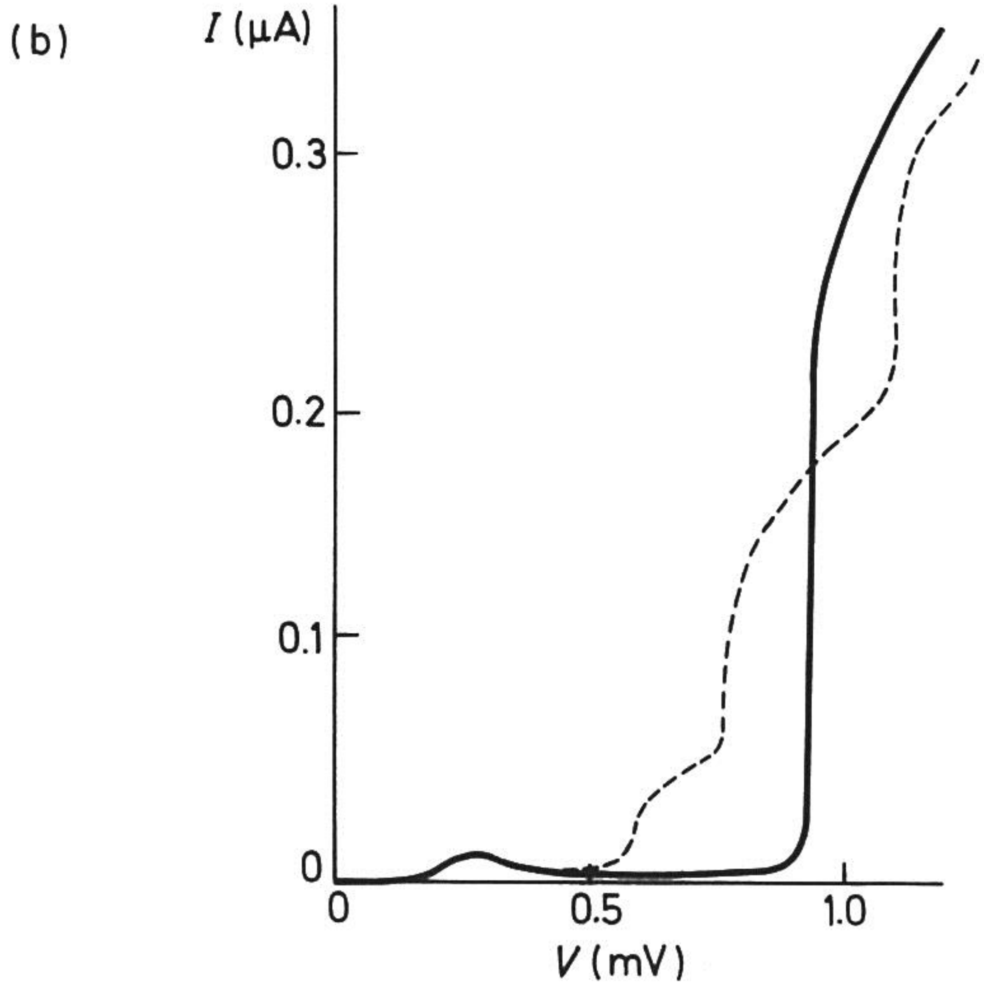

Fig. 5.9 (*b*) Theoretical curves by Tien and Gordon [58] for $\alpha = 2$.

To prove the point that it is the spatial variation which is responsible for the discrepancy, Hamilton and Shapiro [135] conducted another series of experiments on a very small (hardly overlapping in an in-line geometry) junction. The results then did agree with the Tien–Gordon theory as shown in Fig. 5.15.

Two more proofs in favour of the Tien–Gordon theory are the measurements of Hamilton and Shapiro [135] at 200 Hz where V_{rf} could be easily measured and the microwave experiments of Longacre and Shapiro [137] conducted on point contact (that is, very small) junctions.

Shapiro steps to the nth order

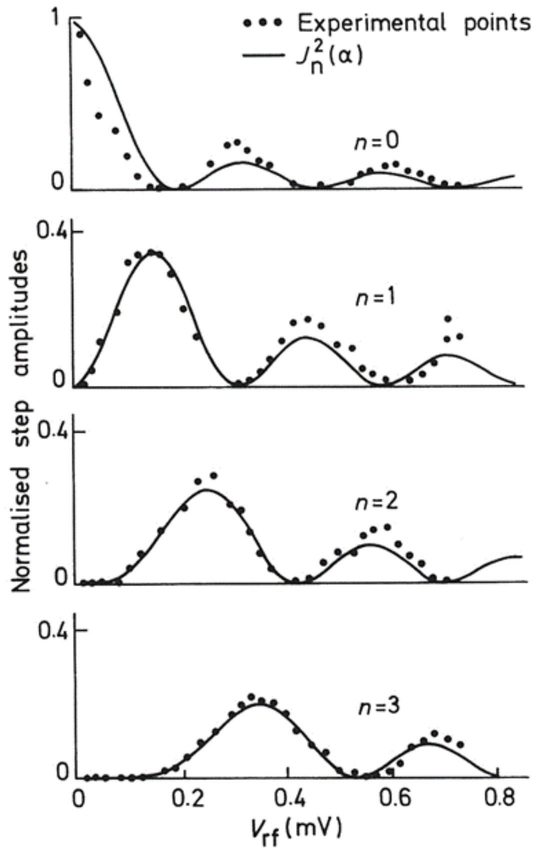

Fig. 5.15 Same as Fig. 5.14 for a very small junction. After Hamilton and Shapiro [135].